Earth Planet. Sci. Lett., 614, 118212, doi:10.1016/j.epsl.2003.118212, 2023.

Interference of ocean and land mass changes in seasonal crustal deformation of coastal stations: A case study in northern Australia

[1,2]Shuo Zheng, [3,4]Kosuke Heki, [1,5]Zizhan Zhang, [4]Yuta Tokui, and [1]Haoming Yan

[1]State Key Laboratory of Geodesy and Earth's Dynamics, Institute Geodesy Geophysics, Chinese Acad. Sci., Wuhan, China
[2]University of Chinese Acad. Sci., Beijing, China
[3]Shanghai Astronomical Obs., Chinese Acad. Sci., Shanghai, China
[4]Dept. Earth Planet. Sci., Hokkaido Univ., Japan
[5]Hubei Luojia Laboratory, Wuhan, China

Highlights

1. Tropical coastal GNSS stations move landward in rain seasons,
2. Northern Australia behaves oppositely
3. Gulf of Carpentaria shows larger mass changes than land hydrology
4. Interference of ocean and land causes opposite phase lags in horizontal and vertical

Abstract

In tropical regions, alternation of rainy and dry seasons causes significant land hydrological mass changes. It brings "landward" seasonal crustal movements of coastal global navigation satellite system (GNSS) stations in rainy seasons. Here, we report that the coastal region of the Gulf of Carpentaria (GOC), northern Australia, behaves oppositely, i.e., they move "oceanward" during austral summer months despite large precipitations on land. Here we study seasonal gravity changes there with satellite gravimetry and analyze seasonal movements of GNSS stations in that region. During the austral summer, hydrological mass increases in nearby land areas. In addition to that, sea water mass within the gulf also increases due to east-southeastward seasonal winds. It has larger amplitudes than on land, and its peak comes a few months earlier, resulting in seasonal displacements of coastal GNSS stations driven predominantly by ocean mass changes. In this study, we emphasize the importance of seasonal horizontal crustal movements, i.e., the oceanward displacements of coastal stations there in austral summer clearly indicate the dominance of the excessive ocean mass over those on land. Such seasonal mass changes within

GOC have been largely overlooked because of insufficient spatial resolution of satellite gravimetry. This study presents a model case for interpreting complicated seasonal surface deformation caused by significant seasonal load changes on land and ocean, often found in coastal areas of half-closed oceans in the world.

1. Introduction

1.1. Crustal deformation by time-variable loads

Hydrological, oceanographic, and atmospheric masses depress the ground and cause crustal subsidence. They also cause horizontal movements toward the loads nearly as large as one third of the subsidence (Farrell, 1972). Changes of hydrological masses such as snowpack, soil moisture, impoundment of reservoirs, cause crustal movements. They often appear in the time series of positions of global navigation satellite systems (GNSS) stations as non-tectonic "noises" with various timescales.

Shortly after the start of the space geodesy era, the importance of crustal deformation signals due to changes in atmospheric loads has been pointed out by van Dam and Wahr (1987). They suggested the possibility of detecting such deformation using techniques such as very long baseline interferometry. Crustal deformation due to hydrological loads have been studied mainly as an important factor responsible for seasonal crustal movements (Dong et al., 2002). For example, seasonal growth of snowpack leaves a strong seasonal signature in GNSS station movements in Japan (Heki, 2001). Crustal deformation due to shorter-timescale hydrological loads has also become a target of geodetic studies. Milliner et al. (2018) and Zhan et al. (2021) studied temporary crustal subsidence due to landfalls of tropical cyclones in North America and in Japan, respectively. Heki and Arief (2022) studied short-term intra-seasonal deformation due to water loads during repeating disastrous rain episodes in SW Japan.

Comprehensive regional studies of various seasonally changing surface loads on land and surrounding oceans have been done in Japan (Heki, 2004), Iceland (Drouin et al., 2016), and worldwide (Dong et al., 2002). GNSS data have been used to estimate change in terrestrial water storages (TWS) (Argus et al., 2014; Jiang et al., 2021; White et al., 2022; Pan et al., 2022). Also, the link of time-variable loads to seismicity has been discussed in regions including Japan (Heki, 2003), Nepal (Bollinger et al., 2007), California (Johnson et al., 2017), and Taiwan (Hsu et al., 2021).

For loads covering large areas, seasonal changes can be also studied using satellite gravimetry by Gravity Recovery and Climate Experiment (GRACE) and its follow-on (GRACE-FO). Seasonal gravity changes are not always consistent with surface movements from GNSS, possibly reflecting the difference in spatial scales of the load the two data sets represent (e.g., Zhang et al., 2021). Nevertheless, comparison of GRACE and GNSS data in seasonal time scale provides important insights into the seasonal mass fluctuations as we show in this study.

1.2. Seasonal movements of coastal stations

Such time-variable loads, except those by tides, are weaker in oceans due to higher mobility of water within the sea. However, significant seasonal mass changes may occur in oceanic regions surrounded by lands as reported for the Red Sea. Its seasonal mass changes were first studied by GRACE gravimetry (Wahr et al., 2014), which motivated the study of seasonal crustal movements of GNSS stations around this sea (Alothman et al., 2020).

The Red Sea is surrounded by arid terrains of the Sahara Dessert and the Arabian Peninsula. Hence, the ocean mass changes govern seasonal movements of GNSS stations on its coast. The situation is opposite in tropical regions. There, rain and dry seasons come in turn, resulting in excess TWS in the former season. Because sea water mass in open oceans generally changes less, seasonal movements of coastal stations are controlled by mass changes on land. Figure 1 shows that tropical coastal GNSS stations move landward in rain seasons and oceanward in dry seasons. The ratio between the amplitudes of the displacements and mass changes varies depending on local situations. For example, displacements of CAL3, Peru, are due mainly to mass changes in the Amazon Basin, located away from the Pacific coast. Hence, its seasonal displacement amplitude is larger than other stations, i.e., 0.45 mm displacement occurs for only 1 cm changes in equivalent water thickness (EWT). This ratio is twice as large as other typical coastal stations such as KOUG, CHPI and YKRO (Figure 1).

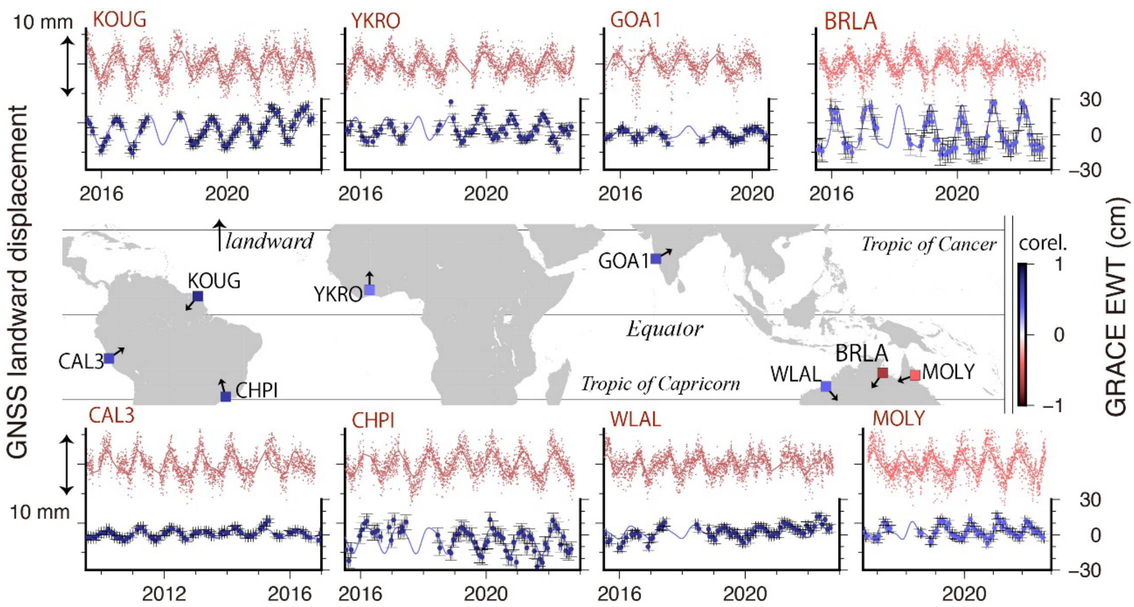

Figure 1. Seasonal landward movements of eight coastal GNSS stations in tropical regions (red, data from Univ. Nevada Reno, see Section 2.1) and mass changes of GRACE mascon on which the GNSS stations reside (blue) over recent years. Arrows attached to the GNSS stations in the map indicate the landward directions, defined as directions roughly perpendicular to regional coastline azimuths. Colors of the stations indicate the correlation

coefficients between the landward displacement and the land mass changes (blue: positive, red: negative). We recognize positive correlations prevail although the ratios between these quantities vary reflecting the areal extent of seasonally changing land mass and its distance from the station. Only the BRLA and MOLY stations, northern Australia, show negative correlations (shown with bright colors).

1.3. Northern Australian coast

Figure 1 shows that the station BRLA, within the Gulf of Carpentaria (GOC), northern Australia, show strong negative correlation between the landward displacement and hydrological mass change on land. Considering that large land hydrological mass changes exist in this region, another seasonally changing masses with a larger amplitude would drive the seasonal displacements of BRLA. Another station in northeast (NE) Australia (MOLY) also shows significant phase difference between landward displacements and land mass changes, suggesting a non-straightforward situation there.

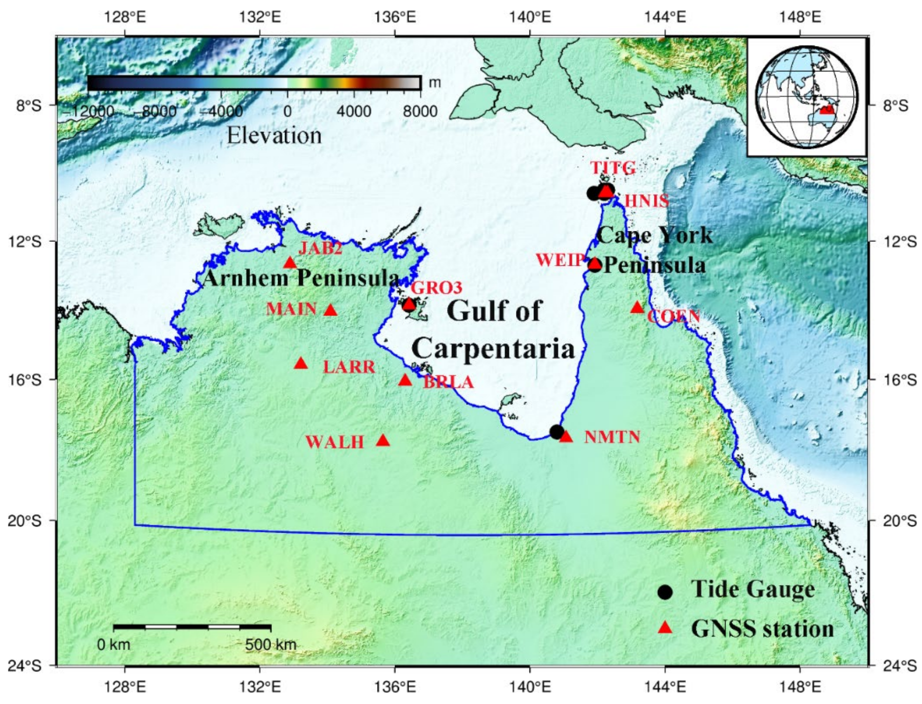

Figure 2. We use GNSS stations (red triangles) and tide gauge stations (black circles) in northern Australia, together with time variable gravity data, to study time-variable mass in GOC and the land area of northern Australia. The thick blue line shows the boundary within which we calculated average land hydrological mass and precipitation in Figure 3.

In northern Australia (Figure 2), the land belongs to tropical rain forests and the alternation of rain and dry seasons makes strong seasonal changes in soil moisture, i.e., the land mass shows maximum in Austral summer months, with the peak in March. GOC is a large oceanic area bounded by the Cape York Peninsula to the east and the Arnhem Peninsula to the west. Tide gauges in this area show strong seasonal change in sea surface height (SSH), i.e., it becomes higher in November-April by tens of centimeters. Wang et al. (2015) suggested such SSH changes are driven by changes in the wind system. This suggests that the SSH changes within GOC are associated with significant water mass changes.

The size of GOC exceeds the spatial resolution of satellite gravimetry. Nevertheless, it is close to the land of Northern Australia where significant hydrological mass changes take place. Moreover, the phases of their seasonal changes are similar, i.e., the peak in SSH comes in January while the peak in land hydrological mass comes in March. Such closeness in phase and space makes data interpretation difficult, and the mass changes in GOC were often interpreted as the leakage from land and/or an artifact due to inaccurate ocean tidal models in GOC (e.g., Dobslaw et al., 2019).

Here we study three-dimensional displacement of GNSS stations along the GOC coast, together with satellite gravimetry and tide gauge data, and land hydrological models. The horizontal components of the displacements would be sensitive to the azimuth of the major load around the stations and help us separate contributions from the loads on land and in ocean.

2. Data and methods

2.1. Continuous GNSS data and processing

We obtain 11 continuous GNSS station time series near GOC spanning the period of 2012–2021 from Nevada Geodetic Laboratory, University of Nevada at Reno (UNR) (Blewitt et al., 2018). In this study, we focus on seasonal components caused by changing oceanic and hydrological loads. We used the GNSS sites whose data span >4 years and with data loss not exceeding 40% (Blewitt & Lavallée, 2002; Yan et al., 2019). To study the ocean mass loading signal in the time series, we corrected for the atmospheric loading displacements in the GNSS data processing (Figure S1) from the Earth System Modeling group at Deutsches GeoForschungs Zentrum (ESMGFZ, http://esmdata.gfz-potsdam.de:8080/repository). Although ocean tidal loading model of GOC adopted in the UNR data base may not be accurate enough, it would not affect daily average station positions. We did not correct for non-tidal ocean loading because that is the target of the present study.

We model the three-dimensional (3D) displacement time series of GNSS stations with offsets, long-term linear trends, annual and semiannual terms, instrumental jumps using the least-squares method assuming the equation (1) (Zhang et al., 2021; Li et al., 2021). There we also consider small jumps and postseismic transients associated with the 2018 February 25 earthquake in Papua New Guinea (M7.5).

$$x(t_i) = x_0 + v(t_i - t_0) + \sum_{j=1}^{2}\left[S_j\, sin(\omega_j t_j) + C_j\, cos(\omega_j t_j)\right] + \sum_{m=1}^{k} E_m H(t_i - t_m) + \sum_{n=1}^{l}\left[H(t_i - t_n)\rho_n log\left(1 + \frac{t_i - t_n}{\tau}\right)\right] + r_i \qquad (1)$$

There, x_0 is the offset, t_0 is the origin of time, v is the long-term velocity, and S_1, C_1 and S_2, C_2 represent the amplitude of annual and semiannual components, respectively. H is the step (Heaviside) function, E is the co-seismic jump at epoch t_m, the occurrence times of earthquakes. ρ indicates the amplitude of the postseismic movements, and t_n indicate the start times of postseismic transients. The relaxation time of the postseismic transients τ was assumed as 67 days. The variable r represents the error.

Next, we remove the estimated offsets, long-term trends, seasonal terms, instrumental and coseismic offsets, and postseismic terms to obtain the residual time series and perform principal component analysis (PCA) on the residual time series to characterize the common mode error (CME) (Dong et al., 2006). After removing CME from the raw time series, we estimate all parameters again using the least-squares method. We fill gaps in data with GNSS Missing Data Interpolation Software (GMIS) based on the Kriged Kalman filter (Liu et al., 2017).

2.2. Satellite gravity data

We used the GRACE and GRACE-FO (called just GRACE hereinafter) version 2 mascon solution (Save et al., 2016; Save et al.,2019), provided by the Center for Space Research (CSR), University of Texas at Austin, represented for $0.25^{\circ} \times 0.25^{\circ}$ latitude-longitude grid to model the seasonal 3D displacements as an elastic response to the changing surface mass.

To reduce the leakage between land and ocean signals, the CSR mascon adopt newly designed hexgonal tiles, and those spanning the coastline are divided into two (land and ocean) tiles. We selected the CSR mascon solution because of its small tile sizes, but confirmed that using other solutions (e.g., Jet Propulsion Laboratory mascon) does not influence the final conclusion of this study. We use these mascon data to investigate time-variable loads around GOC. We calculate the 3D displacement field from the GRACE data as follows (Farrell, 1972):

$$E(\theta,\varphi) = -\iint sin\,(A)\Delta m(\theta',\varphi')G_H(\psi)cos(\varphi')d\,\theta' d\varphi' \tag{2}$$

$$N(\theta,\varphi) = -\iint cos\,(A)\Delta m(\theta',\varphi')G_H(\psi)cos(\varphi')d\,\theta' d\varphi' \tag{3}$$

$$U(\theta,\varphi) = \iint \Delta m(\theta',\varphi')G(\psi)cos(\varphi')d\,\theta' d\varphi' \tag{4}$$

Where Δm represents the mass change at cell (θ',φ'), $G(\psi)$ and $G_H(\psi)$ are the vertical and horizontal Green's functions (Wang et al., 2012), respectively. ψ is the angular distance between the (θ',φ') and the (θ,φ). $E(\theta,\varphi)$, $N(\theta,\varphi)$, and $U(\theta,\varphi)$ are the three components of the elastic displacement vector at coordinate (θ,φ) caused by the mass at (θ',φ'). A indicates the azimuth, measured clockwise from the local north to the mass. In these calculations, we only used regional mass changes after confirming that large seasonally changing mass in far-fields, such as High Mountain Asia, causes only insignificant displacements for GNSS stations around GOC.

2.3. Hydrological model

We use monthly TWS estimates from the Global Land Data Assimilation System (GLDAS) Noah hydrological models given at spatial grids of $0.25^{\circ} \times 0.25^{\circ}$ extending from 180.0°W to 180.0°E and 60.0°S to 90.0°N, developed by NASA Goddard Space Flight Center (GSFC) and NOAA National Centers for Environmental Prediction (Rodell et al., 2004). The monthly TWS estimates from these models are calculated by summing monthly average soil moisture (2 m column depth), total canopy water storage, and water equivalent snow depth, and cover the period 2012-2021.

2.4. Tide gauge data

In this work, we obtained monthly SSH data at 6 tide gauge stations along the coast of GOC from the Permanent Service of Mean Sea Level (PSMSL). Tide gauge observations provide an independent measure of SSH anomalies to validate the significant seasonal changes of seawater mass in GOC. In order to compare with the GRACE estimates, we considered the thermosteric effects in the tide gauge observations using the Estimating the Circulation and Climate of the Ocean (ECCO) model. We did not correct for the seasonal vertical crustal movements at the tide gauge stations considering their amplitudes are smaller, by an order of magnitude, than those of the seasonal SSH changes there.

3. Results

3.1. Seasonal mass changes in and around GOC from GRACE data

First, we compare the monthly mean SSH values of the 7 tide gauge data and those inferred as EWT from the GRACE data in GOC (Figure 3). Because the tide gauge data include steric components, the figure also includes a curve showing the GRACE data after adding seasonal steric components derived from the ECCO models. We find that both show significant seasonal changes. In comparison with the tide gauge observations, the amplitudes of the seasonal changes in the GRACE data, with and without thermosteric corrections, are somewhat smaller. Their phases are mostly coherent, with the difference not exceeding 1 month.

Figure 2 shows that the tide gauges used in this study are distributed mostly along the eastern coast of GOC (i.e., western coast of the Cape York Peninsula). Hence, it is likely that the mean value of the tide gauge observations reflects SSH in the eastern GOC. Figure S2 compares the amplitudes of SSH from individual tide gauges. There, the seasonal amplitudes significantly differ between those on the eastern (KARUMBA/WEIPA) and the western (MILNER BAY) coasts of GOC. It is also clear that the amplitudes are larger at stations deeper inside the gulf. Such differences are reasonable considering that these changes are driven by seasonal winds, i.e., strong winds toward east-southeast

(ESE) elevates the winter SSH within GOC (Wang et al., 2015). This suggests that average seasonal SSH changes (Figure 3) are biased to the eastern GOC, which would partly explain the larger tide gauge amplitude than GRACE.

On the other hand, GRACE estimates of mass changes, averaged over the land area (spatial extent indicated in Figure 2), have amplitudes about two-thirds of those of GOC. Its peak comes a few months later than GOC, i.e., the maximum occurs in March and the minimum occurs in September-October. These peak months correspond to the ends of the rain and dry seasons (see precipitation in Figure 3). The dominance of land and ocean excess masses switches in April and September, i.e., the land and ocean masses are dominant in May-August and October-February, respectively. Such an alternating dominance should appear in the azimuths of horizontal seasonal displacements of GNSS stations around GOC, i.e., they would move landward and oceanward in these months, respectively.

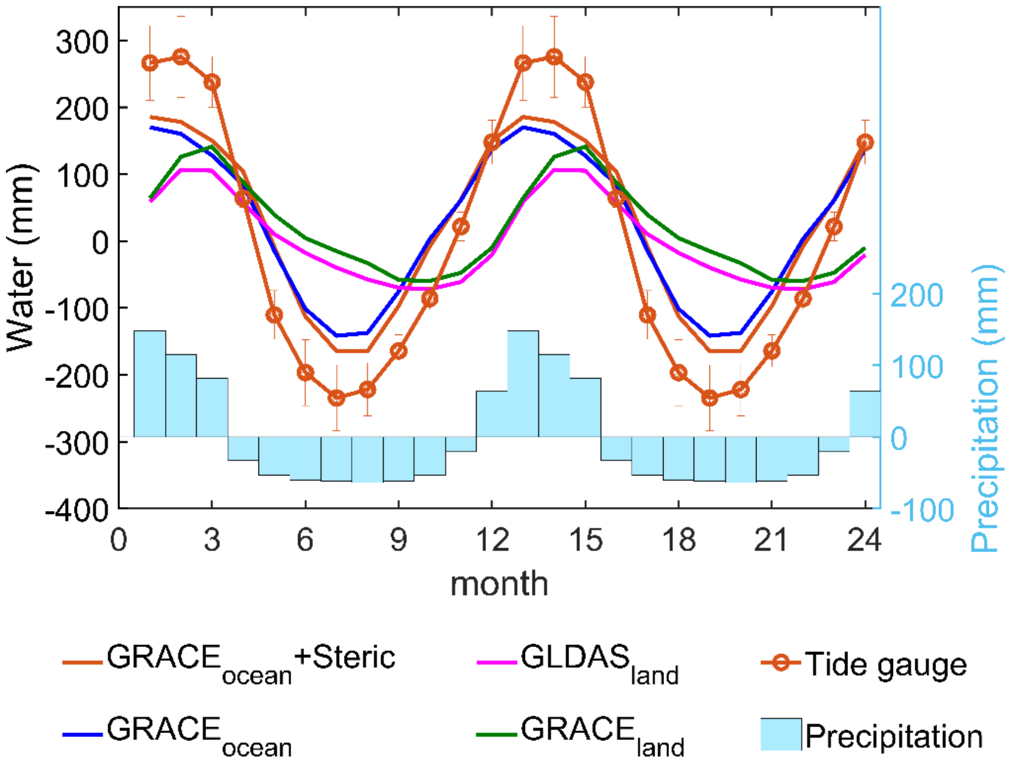

Figure 3 Comparison of seasonal (monthly mean) changes of SSH from tide gauges (averages of all the points in Figure 2, with error bars showing standard deviations), mass changes in ocean (GOC, averaged over 136-142E, 17.5S-10.0S), with and without corrections for thermosteric changes, and the land area surrounding GOC, from GRACE, and from the GLDAS model. We also show monthly average land precipitation (over the same region as GRACE data, see Figure 2) as the deviations from the whole year average with light blue bars (from the ECMWF reanalysis model over 2012-2021). The land GRACE/GLDAS values were obtained by averaging the region surrounded by the blue line in Figure 2.

3.2. Seasonal crustal movements of GNSS stations located between two loads

Figure 3 shows that seasonal mass changes are significant both in GOC and its adjacent land area. The amplitude is somewhat larger in the ocean than on land. As shown in Figure 1, this is a rare case considering that, in most tropical regions, mass changes in oceans are less than those on lands, and seasonal crustal movements of coastal GNSS stations are governed by land hydrology. In and around GOC, comparable amplitudes of seasonal mass changes occur both on land and ocean, and they have a phase shift, i.e., the peak comes a few months earlier in ocean.

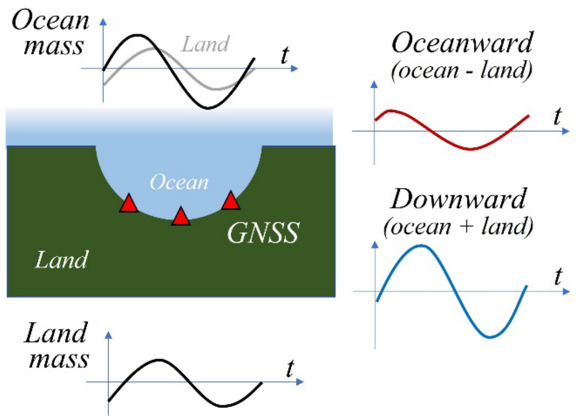

Figure 4 Concept of two masses, ocean and land, whose seasonal changes are significant and have a phase shift. The horizontal movement of a coastal GNSS stations reflects the difference of the contributions from the two masses while the vertical component reflects their sum. As a consequence, peaks of the downward and oceanward displacements slightly deviate to later and earlier months.

Here we discuss how coastal GNSS station behave in such a case. Figure 4 models the situation in GOC. Ocean and land masses change seasonally, and the former has a larger amplitude and an earlier peak month. There, vertical crustal movements reflect the “sum” of the land and ocean loads. In contrast, horizontal displacements tend to the dominant load, i.e., they reflect the “difference” between the two loads. We should note such different behaviors of the vertical and horizontal displacements.

Actually, displacements are the integration of contributions from individual point masses over finite regions. In the GOC case, seasonal change amplitudes and area covered by the loads are comparable for the ocean and the land. Clear negative correlation between landward displacements and land mass changes at BRLA (Figure 1) suggests that the land load is not dominant. In other words, seasonal movements of coastal GNSS stations are governed by the ocean load. Nevertheless, influences of the land mass do emerge as the shifts of peak months of the seasonal displacements as illustrated in Figure 4. The peak of the horizontal movements, representing the difference between the land and ocean mass, would shift to an earlier month. On the other hand, the peak month of the subsidence, representing the sum of the two masses, would shift to a later month. According to a simple numerical simulation, if the phase shift between the ocean and the land mass is 2 months and the displacement by the latter is 2/3 of the former, the phase advance of the oceanward displacement is a little more than 1 month and the phase delay of the subsidence is a little less than 1 month.

3.3. Observed seasonal movements of GNSS station

Here, we discuss the 3D seasonal movements in 2012-2021 observed at eleven GNSS sites in northern Australia surrounding GOC (Figure 2). Figure 5 shows monthly displacements relative to the average positions (hence, apparent uplifts occur in months with less loads). Their amplitudes are a few mm in horizontal, but the peak-to-peak changes, i.e., the difference between the maximum and the minimum, are nearly 1 cm in vertical. They change seasonally suggesting that they are driven by seasonal mass changes in this region. Figure 5 show both observed and modeled movements. To clearly visualize the observed movements, only the observed vectors are shown in Figure S3.

An important feature in the horizontal movements is the reversal of the displacement azimuth between two periods, austral winter-spring (July-November) and summer-autumn (January-May). GNSS stations move away from/towards GOC in the former/latter periods. Vertical components show similar changes in polarities, they show subsidence and uplifts (relative to averages) in these seasons, respectively. In June and December, such movements are not clear. Instead, we see eastward and westward movements of the whole region in these months. Vertical components are neutral in these two transition months.

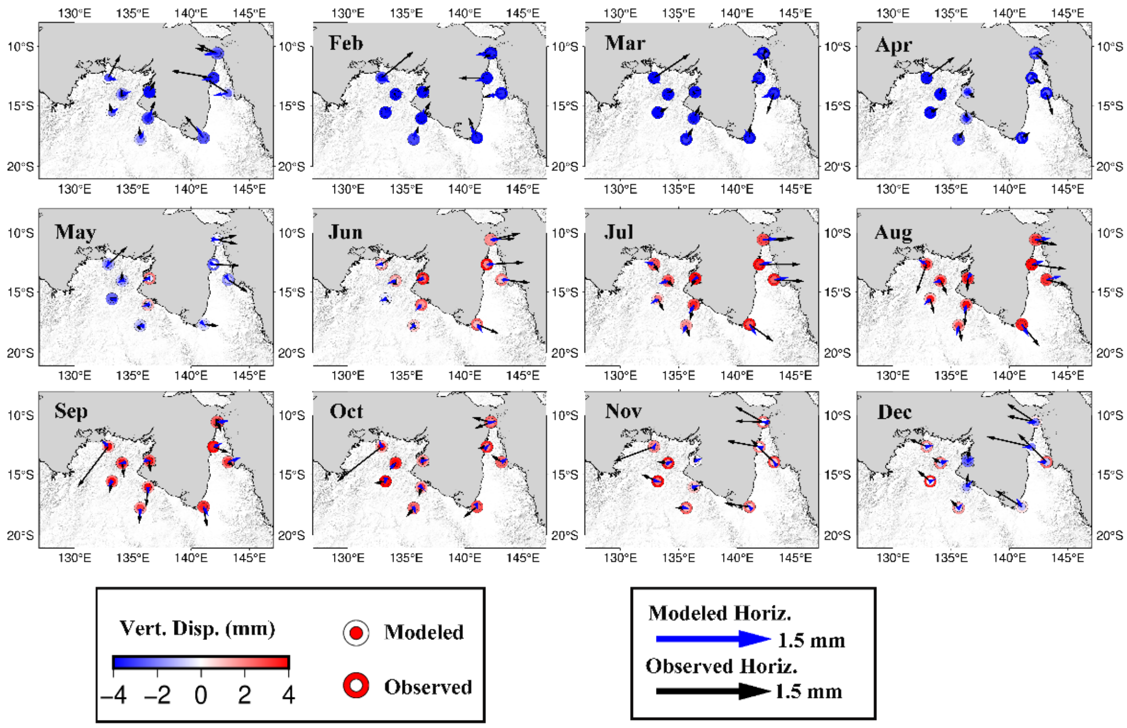

Figure 5 Observed and modeled (calculated) seasonal (monthly mean) horizontal crustal movements of GNSS stations around GOC for the period 2012–2021. Arrows represent observed monthly mean horizontal displacements, and colors of circles represent vertical displacements. They are both relative to the average positions.

The polarity changes of the vertical components are consistent with the mass changes in GOC, but its peak subsidence/uplift in March/September comes slightly later than the GOC mass peak/valley. This phase delay is predicted in Figure 4 and is shown as time series in Figure 6a. Regarding the horizontal component, the peak oceanward displacement occurs earlier than the peak GOC mass. Such a phase shift agrees with the prediction in Figure 4 and is shown as time series of oceanward displacements in Figure 6b. As a whole, the 3D seasonal displacement of GNSS stations around GOC are largely controlled by the GOC mass changes. However, the subsidence and oceanward displacement peaks occurs later and earlier, respectively, than the GOC mass peak due to interference with the mass changes on land. The phase shifts for the vertical and horizontal displacements are opposite because the former reflects the sum, and the latter reflects the difference between the two masses.

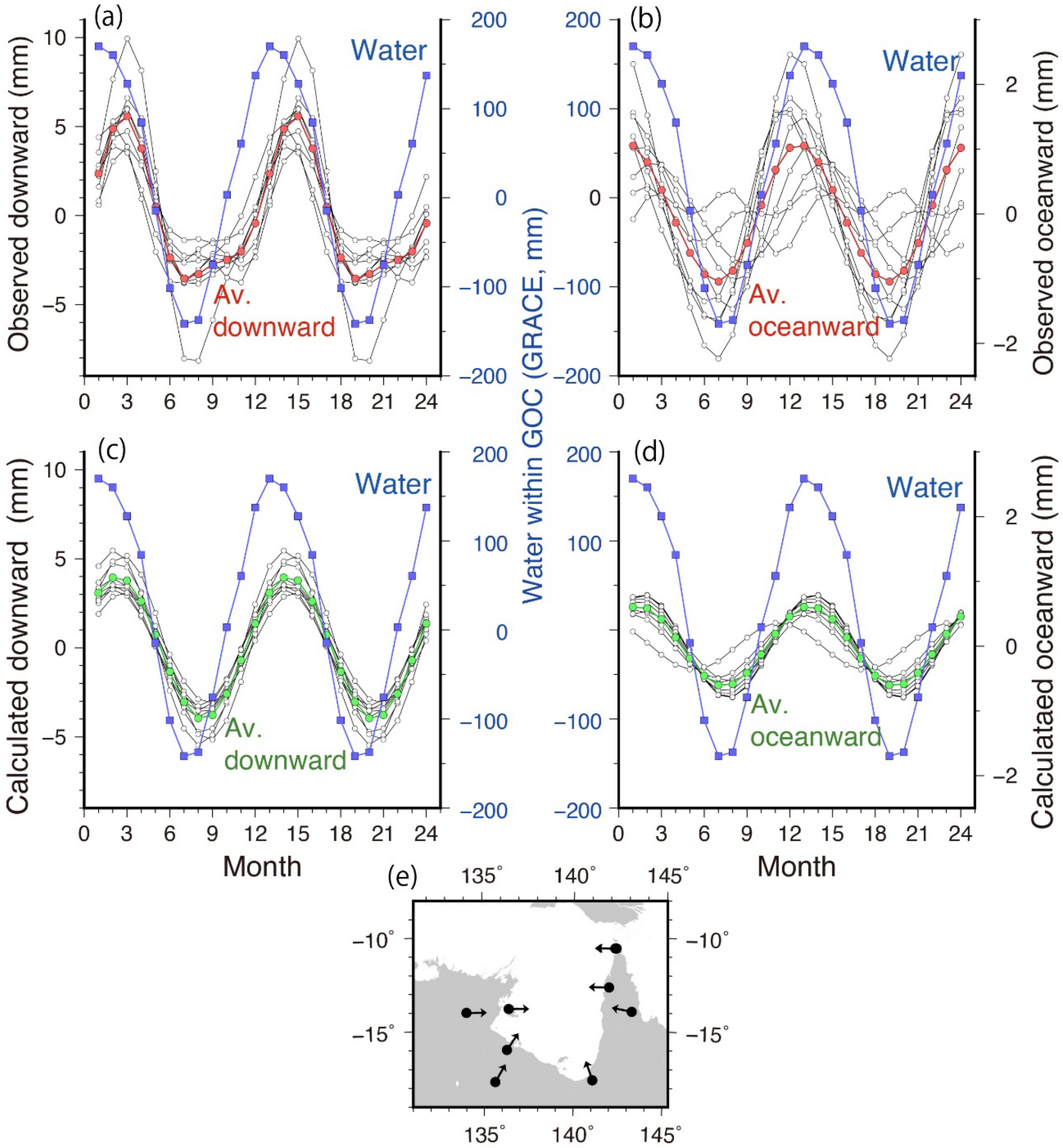

Figure 6 (a) Monthly average downward observed seasonal displacements for 9 GNSS stations around GOC (thin black lines) and their average (red). We excluded two stations, JAB2 and LARR, deep in the Arnhem Peninsula. (b) Observed oceanward monthly average displacements for the 9 stations. "Oceanward" directions are defined by arrows attached to the GNSS stations in (e). Blue curves in (a-d) represent average seasonal water thickness changes within GOC observed by GRACE (same data as in Figure 3).

Although seasonal displacements of coastal GNSS stations are governed by GOC seawater mass changes, the phase delay and advance occur in the vertical and horizontal components, respectively, due to interference with land mass changes. The observed phase delay and advance of individual stations mostly fall in the range from one to two months, which is consistent with the expectation (Figure 4). The observed downward and oceanward displacements have peak-to-peak amplitudes of ~9.1 mm and ~2.1 mm, respectively.

(c) and (d) show modeled downward and oceanward, respectively, monthly average seasonal displacements for the same 9 GNSS stations around GOC, calculated using GRACE monthly mass anomalies (Figure 7), and their averages (green). The phase delay and advance from the GOC water level are mostly consistent with the observed displacements in (a) and (b). Average calculated downward and oceanward displacements have peak-to-peak amplitude of ~7.9 mm and ~1.2 mm, respectively, which is somewhat smaller than the observed amplitudes shown in (a) and (b).

Another interesting feature in Figure 5 is the behavior of the GNSS points near the northern tip of the Cape York Peninsula. They move by 1-2 mm eastward/westward, i.e., toward the Pacific Ocean and GOC, in April-August/October-February. The peak eastward/westward displacement occurs in June/December, the neutral months of the horizontal displacements of stations around GOC. At these stations, changes in the continental hydrological mass plays a minor role, i.e., these movements are driven mostly by the ocean load contrast between the eastern (Pacific Ocean) and western (GOC) oceans. Because the former is much smaller, these movements simply reflect mass changes in GOC and its phase coincides with the GOC mass changes (Figure 3). We will discuss this matter later in Section 4.2.

4. Discussion

4.1. Mass changes and the seasonal crustal movements: GOC

Wang et al. (2015) showed that annual sea level variations along the northern Australian coast are driven by seasonal winds. Figure 7 shows monthly average surface winds at grid points with arrows. From December to March, the west-northwest winds (east-southeastward winds) prevail in GOC, and the sea water blown into GOC increases the water mass there. On the other hand, east-southeast (west-northwestward) wind prevails from April to November, which let the GOC water mass decrease.

In order to compare with the observed seasonal crustal movements, we calculated monthly displacements of GNSS stations using seasonal loads observed by satellite gravimetry. Figure 7 shows monthly GRACE mass deviations from annual averages, and corresponding displacements (arrows in Figure 7) calculated using equations (2)-(4), and the Green's function by Wang et al. (2012). They show fairly good consistency with the observed horizontal displacements (Figure 5). The horizontal displacements are oceanward in austral summer-autumn and landward in austral winter-spring. Regarding the vertical, subsidence prevails in the former season and vice versa.

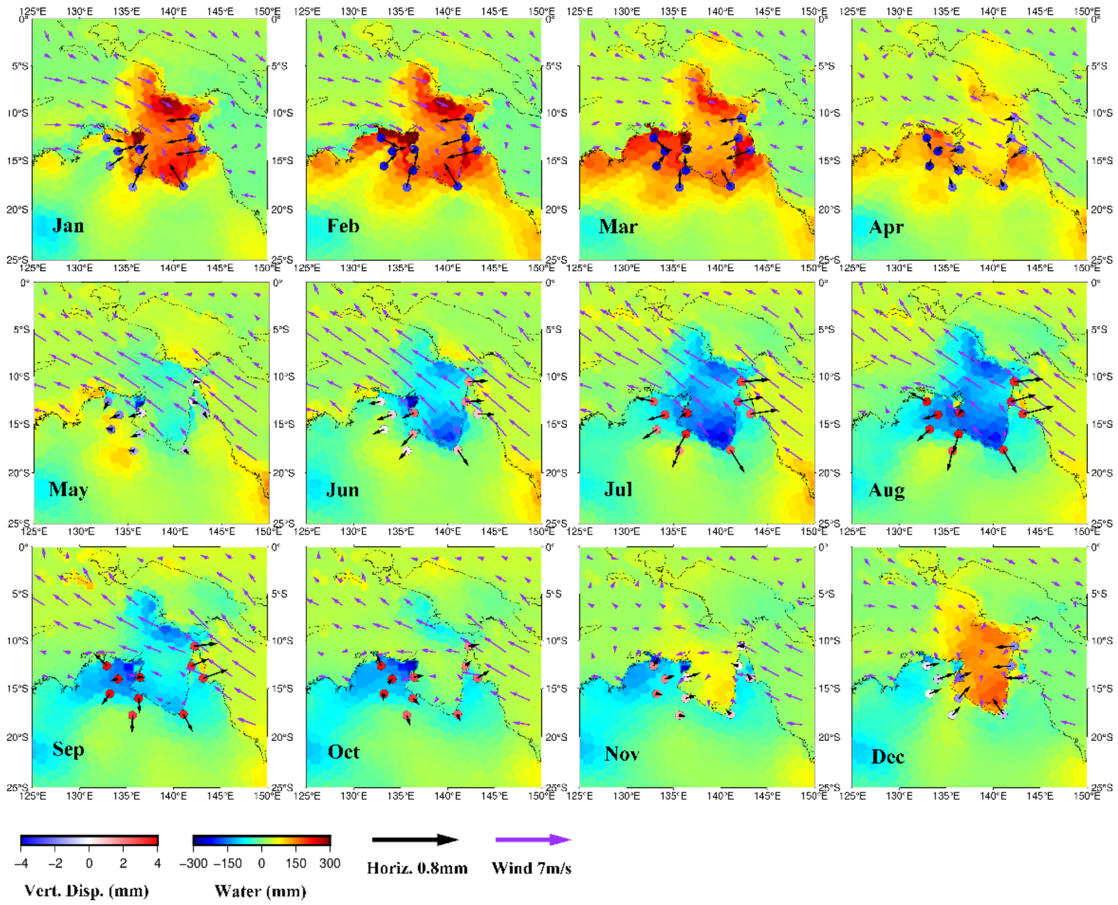

Figure 7 Monthly average surface wind vectors from the ECMWF reanalysis model in the oceanic area (thin gray arrows), seasonal mass anomalies from GRACE (red and blue indicate mass excess and deficit, respectively), and the 3D displacements of the GNSS stations calculated using the GRACE mass anomalies.

Figure 6c,d compiles calculated downward and oceanward monthly displacements in the same way as the observed displacements in Figure 6a,b. Significant discrepancy in amplitude is often observed when we compare GNSS displacements and GRACE time-variable gravity data due to the difference in the area represented by GNSS and GRACE data (e.g., Zhan et al., 2021). However, the average peak-to-peak amplitude of the observed vertical displacements is 9.1 mm (Figure 6c), and this is only slightly larger than the calculated amplitude of 7.9 mm (Figure 6a).

The difference is a little more significant for the horizontal component. The average peak-to-peak amplitude of the observed oceanward/landward displacements is 2.1 mm (Figure 6d), which is larger than the calculated amplitude of 1.2 mm (Figure 6b). This difference is <1 mm but is nearly two in factor. Regarding the phases, the calculated and observed changes are mostly consistent, i.e., the downward peaks come slightly later than the GOC water mass peaks (the oceanward peak should come a little earlier than GOC but it is not so clear as in Figure 6b). The discrepancy in amplitude for the horizontal may reflect the insufficient spatial resolution of mass distribution in the GRACE mascon solution. The discrepancies are larger at GNSS stations within the Arnhem Peninsula (Figure 5), and this would reflect the larger difference of the mass anomalies by GRACE on land from the reality.

4.2. Mass changes and the seasonal crustal movements: The Cape York Peninsula

As shown in Figure 5, most GNSS stations show eastward/westward displacements in June/December. This is well reproduced in the calculation for stations in the northern part of the Cape York Peninsula (Figure 7). These stations are relatively insensitive to continental hydrological mass changes that suffer uncertainties due to insufficient spatial resolution of the GRACE data. Hence, their movements would mainly reflect ocean mass contrast between the two sides of the peninsula. Both the observed and calculated horizontal displacement vectors show a reversal of horizontal displacement azimuth between April-August (eastward) and October-February (westward). Considering the nearly constant ocean mass on the Pacific Ocean side, this would be driven by the ocean mass changes within GOC.

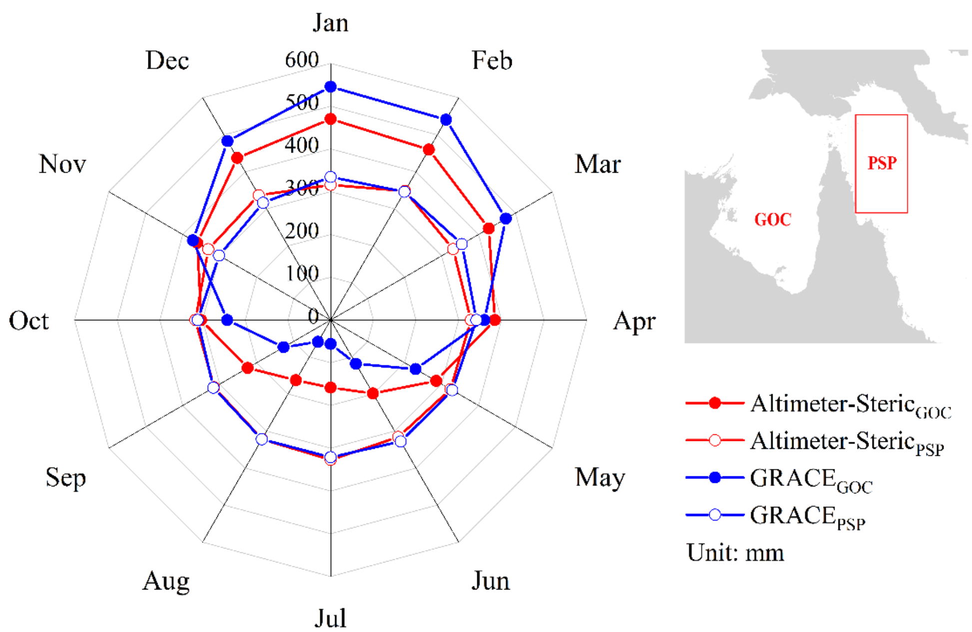

Figure 8 The area-average ocean mass anomalies calculated with the GRACE data (blue) and the SSH anomalies (after steric corrections) from altimetry (red) are compared between the Pacific side of the peninsula (PSP, see the inset map for the area it represents) and in the GOC.

In Figure 8, we show area-averaged seasonal ocean mass anomalies from GRACE and the altimetric SSH anomalies in the oceans at the two sides of the peninsula. A seasonal fluctuation with an amplitude of ~310 mm occurs in GOC, but it is only ~35 mm at the Pacific side. Mass decreases significantly in GOC during May-September, while it keeps stationary on the Pacific side. Altimetry also shows similar seasonal changes to GRACE. Steric correction makes it inconsistent, suggesting a larger errors in seawater temperature profile within the gulf. The largest westward displacement occurs in January, and this is consistent with the seasonal changes from GRACE and altimetry.

4.3. Seasonal crustal movements by multiple sources of mass changes: Perspectives

Here we studied ocean mass changes in and around GOC, northern Australia, and using data from multiple sensors. Seasonal mass changes in GOC were largely responsible for the seasonal displacements of coastal GNSS stations in this region. In tropical regions, land hydrological mass usually governs seasonal movements of coastal GNSS stations (Figure 1). This makes the studied area unique. Before concluding our study, we discuss if such areas are to be found in other parts of the world.

One such candidate is the Gulf of Thailand (GOT), Southeast Asia, located to the southwest of the South China Sea and surrounded by Thailand, Cambodia, and Vietnam. The GRACE data shows that seasonal mass changes within GOT have a peak-to-peak amplitude exceeding GOC. The peak in GOT comes several months later than on land (e.g., Thailand). Therefore, coastal GNSS stations around GOT would show complicated 3D seasonal displacements reflecting interference of seasonal mass changes on land and ocean. Unfortunately, we do not have GNSS stations at right places covering enough time with sufficient density, to confirm them.

In the arid region, in addition to the Red Sea discussed in the introduction, smaller but significant seasonal mass changes may occur in the Persian Gulf, driving seasonal crustal movements of coastal GNSS stations there. In mid-latitude regions, GRACE and altimetry data show that significant seasonal water mass changes with peak-to-peak amplitude of ~10 cm may occur in the Japan Sea (e.g., Heki and Yi, 2018). However, the northeast Japan has a strong seasonal signal from snowpack (e.g., Heki, 2004), and it would not be easy to isolate the ocean signal in seasonal displacements of coastal GNSS stations there. GNSS stations on the continental side of the Japan Sea coast will help us study them.

5. Conclusions

Our study clarified the mass changes and displacements in and around GOC, northern Australia.

(1) In northern Australia, significant seasonal mass changes occur on land, but stronger changes of a few tens of centimeters also occur within GOC.

(2) Seasonal mass changes in GOC from GRACE are driven by seasonal winds, and its amplitude is ~1.5 times as large as the hydrological mass changes in the surrounding land area.

(3) Seasonal movements of GNSS stations around GOC are governed by GOC mass changes in polarity, i.e., oceanward/subsidence in austral summer and autumn, and landward/uplift in austral

winter and spring. However, its phase shifts by 1-2 months due to interference with the seasonal land mass changes.

(4) Seasonal horizontal crustal movements in east-west direction of GNSS stations near the northern tip of the Cape York Peninsula are driven by the ocean mass contrast between the eastern (the Pacific Ocean) and the western (GOC) sides.

(5) This study provides a unique case of seasonal crustal deformation in a tropical area driven by ocean mass in addition to land hydrology. Seasonal crustal deformation driven by ocean loads has not been fully explored and includes future targets of investigation in the world.

Acknowledgments. The GNSS daily coordinates used in this study are available from the Nevada Geodetic Laboratory, University of Nevada, Reno (geodesy.unr.edu/gps_timeseries/tenv3/IGS14). The CSR GRACE products used in the study were downloaded from www2.csr.utexas.edu/grace/. GLDAS data is available at https://disc.gsfc.nasa.gov/. The ERA5 rainfall and wind reanalysis dataset is available from the Copernicus Climate Data Store (cds.climate.copernicus.eu/cdsapp#!/home/). The satellite altimeter sea surface height data are available from the COPERNICUS Marine Environment Monitoring Service (http://marine.copernicus.eu/). The tide gauge data are available from psmsl.org/data/. The project is funded by the NSFCs (Grant Nos. 41874098, 42174042 and 42174100), the Open Fund of Hubei Luojia Laboratory (220100044), and Chinese Academy of Sciences, President's International Fellowship Initiative (Grant 2022VEA0014). We thank Yuanjin Pan and an anonymous reviewer for constructive comments.

References

Alothman, A.O., Bos, M., Fernandes, R., Radwan, A.M., Rashwan, M., 2020. Annual sea level variations in the Red Sea observed using GNSS. Geophys. J. Int., 221, 826-834, doi:10.1093/gji/ggaa032.

Argus, D.F., Fu, Y., Landerer, F.W., 2014. Seasonal variation in total water storage in California inferred from GPS observations of vertical land motion. Geophys. Res. Lett., 41(6), 1971–1980.

Blewitt, G., Lavallée, D., 2002. Effect of annual signals on geodetic velocity. J. Geophys. Res., 107, 2145. doi:10.1029/2001JB000570

Blewitt, G., Hammond, W., Kreemer, C., 2018. Harnessing the GPS data explosion for interdisciplinary science. Eos, 99.

Bollinger, L., Perrier, F., Avouac, J.-P., Sapkota, S., Gautam, U., Tiwari, D.R., 2007. Seasonal modulation of seismicity in the Himalaya of Nepal. Geophys. Res. Lett., 34, L0804, doi:10.1029/2006GL029192.

Dobslaw, H., Zhang, L., Bagge, M., Dill, R., Klemann, V. and Thomas V., 2019. Separating GRACE-based ocean bottom pressure estimates into wind-driven circulation signatures and spatially variable mass-induced sea-level changes. paper presented at the EGU General Assembly, 7-12 April 2019, Vienna, Austria.

Dong, D., Fang, P., Bock, Y., Cheng, M. K., Miyazaki, S., 2002. Anatomy of apparent seasonal variations from GPS-derived site position time series. J. Geophys. Res., 107, 2075, doi:10.1029/2001JB000573.

Dong, D., Fang, P., Bock, Y., Webb, F., Prawirodirdjo, L., Kedar, S., Jamason, P., 2006. Spatiotemporal filtering using principal component analysis and Karhunen-Loeve expansion approaches for regional GPS network analysis. J. Geophys. Res., Solid Earth, 111. B03405, doi：10.1029/2005JB003806.

Drouin, V., Heki, K., Sigmundsson, F., Hreinsdóttir, S., Ófeigsson, B.G., 2016. Constraints on seasonal load variations and regional rigidity from continuous GPS measurements in Iceland, 1997-2014. Geophys. J. Int., 205, 1843-1858, doi:10.1093/gji/ggw122.

Farrell, W.E., 1972. Deformation of the Earth by surface loads. Rev. Geophys., 10(3), 761–797. doi:10.1029/ rg010i003p00761.

Heki, K., 2001. Seasonal modulation of interseismic strain build-up in Northeastern Japan driven by snow loads. Science, 293, 89-92.

Heki, K., 2003. Snow load and seasonal variation of earthquake occurrence in Japan. Earth Planet. Sci. Lett., 207, 159-164.

Heki, K., 2004. Dense GPS array as a new sensor of seasonal changes of surface loads, in State of the Planet: Frontiers and Challenges in Geophysics, edited by R. S. J. Sparks and C.J. Hawkesworth, Geophysical Monograph Ser. 150, 177-196, American Geophys. Union, Washington.

Heki, K., Arief S, 2022. Crustal response to heavy rains in Southwest Japan 2017-2020, Earth Planet. Sci. Lett., 578, doi:10.1016/j.epsl.2021.117325.

Heki, K., Yi, S., 2018. Seasonal crustal deformation in NE Japan and sea level budget of the Japan Sea. paper presented at the AGU Fall Meeting, Washington DC, Dec. 10-14.

Hsu, Y.J., Kao, H., Bürgmann, R., Lee, Y.T., Huang, H.H., Hsu, Y.F., Wu, Y.M., Zhuang, J., 2021. Synchronized and asynchronous modulation of seismicity by hydrological loading: A case study in Taiwan. Sci. Adv., 7, eabf7282, doi:10.1126/sciadv.abf7282.

Jiang, Z., Hsu, Y.-J., Yuan, L., Cheng, S., Feng, W., Tang, M., Yang, X., 2022. Insights into hydrological drought characteristics using GNSS-inferred large-scale terrestrial water storage deficits. Earth Planet. Sci. Lett., 578, 117294.

Johnson, C.W., Fu, Y., Bürgmann, R., 2017. Seasonal water storage, stress modulation, and California seismicity. Science, 356, 1161-1164.

Li, J., Zhan, W., Guo, B., Li, S., Guo, B., 2021. Combination of the Levenberg–Marquardt and differential evolution algorithms for the fitting of postseismic GPS time series. Acta Geophysica(5–6), doi:10.1007/s11600-021-00556-y

Liu, N., Dai, W., Santerre, R., Kuang, C., 2017. A MATLAB-based Kriged Kalman Filter software for interpolating missing data in GNSS coordinate time series. GPS Solutions 22, doi:10.1007/s10291-017-0689-3.

Milliner, C., Materna, K., Bürgmann, R., Fu, Y., Moore, A.W., Bekaert, D., Adhikari, S., Argus, D.F., 2018. Tracking the weight of Hurricane Harvey's storm water using GPS data. Sci. Adv., 4(9), eaau2477. doi:10.1126/sciadv.aau2477.

Pan, Y., Ding, H., Li, J., Shum, C.K., Mallick, R., Jiao, J., Li, M., Zhang, Y., 2022. Transient hydrology-induced elastic deformation and land subsidence in Australia constrained by contemporary geodetic measurements, Earth Planet. Sci. Lett., 588, doi.org/10.1016/j.epsl.2022.117556

Save, H., Bettadpur, S., Tapley, B.D., 2016. High-resolution CSR GRACE RL05 mascons. J. Geophys. Res., Solid Earth, 121, 7547–7569, doi:10.1002/2016jb013007.

Save, H., 2019. CSR GRACE RL06 Mascon Solutions. Texas data repository Dataverse V1, doi:10.18738/T8/UN91VR.

van Dam, T.M., Wahr, J.M., 1987. Displacement of the earth’s surface due to atmospheric loading – Effects of gravity and baseline measurements. J. Geophys. Res., 92, 1281-1286, doi:10.1029/JB0092iB02p01281.

Wahr, J., Smeed, D.A., Leuliette, E., Swenson, S., 2014. Seasonal variability of the Red Sea, from satellite gravity, radar altimetry, and in situ observations. J. Geophys. Res., Oceans, 119, 5091-5104, doi:10.1002/2014JC010161.

Wang, H., Xiang, L., Jia, L., Jiang, L., Wang, Z., Hu, B., Gao, P., 2012. Load love numbers and Green’s functions for elastic earth models PREM, iasp91, ak135, and modified models with refined crustal structure from crust 2.0. Comput. Geosci. 49, 190–199, doi:10.1016/j.cageo.2012.06.022.

Wang, J., Wang, J., Cheng, X., 2015. Mass-induced sea level variations in the Gulf of Carpentaria. J. Oceanogr., 71(4), 449-461.

White, A.M., Gardner, W.P., Borsa, A.A., Argus, D.F., Martens, H.R., 2022. A review of GNSS/GPS in hydrogeodesy: Hydrologic loading applications and their implications for water resource research. Water Resources Res., 58, doi:10.1029/2022WR032078.

Yan, J., Dong, D., Bürgmann, R., Materna, K., Tan, W., Peng, Y., Chen, J., 2019. Separation of sources of seasonal uplift in China using independent component analysis of GNSS time series. J. Geophys. Res., Solid Earth, 124, 11951-11971, doi:10.1029/2019JB018139

Zhan, W., Heki, K., Arief, S., Yoshida, M., 2021. Topographic amplification of crustal subsidence by the rainwater load of the 2019 typhoon Hagibis in Japan. J. Geophys. Res., Solid Earth, 126,

e2021JB021845
Zhang, L., Tang, H., Sun, W., 2021. Comparison of GRACE and GNSS seasonal load displacements considering regional averages and discrete points. J. Geophys. Res., Solid Earth, 126(8), 1-27, doi:10.1029/2021JB021775.

Supplementary materials

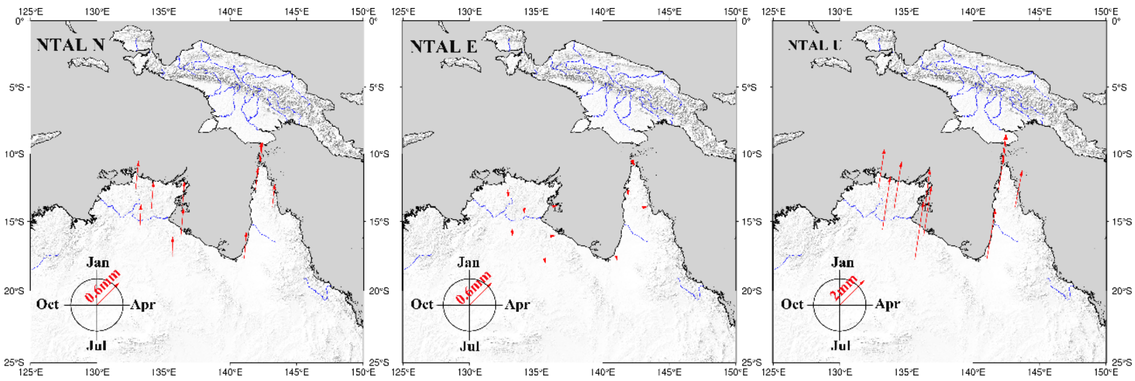

Figure S1. Annual amplitudes and peak phases of non-tidal atmospheric loading (NTAL) displacements at GNSS stations around GOC. The arrows indicate the months when annual deformation reaches the maximum. They are much less than those by hydrological and ocean mass loads.

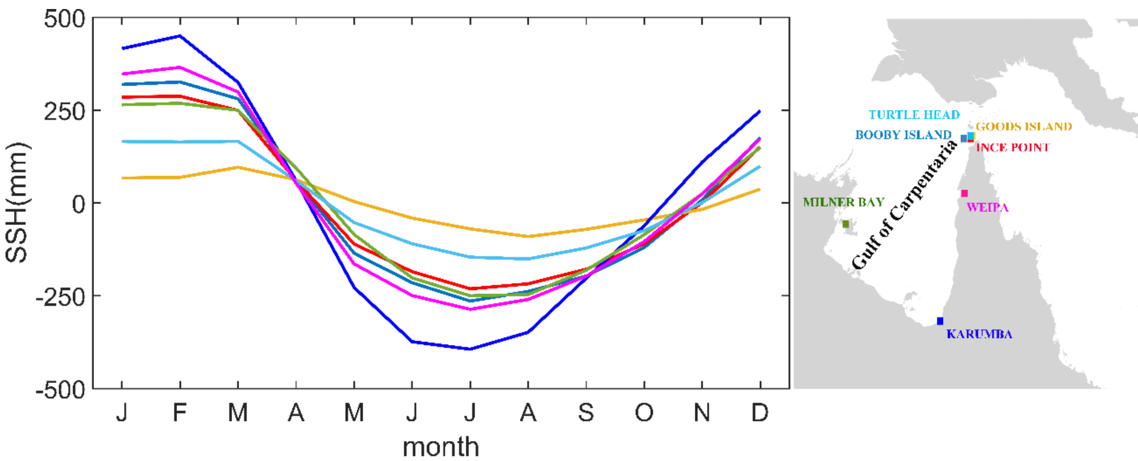

Figure S2 Average monthly changes of SSH from the tide gauges around GOC. Amplitudes become larger as we go deep into GOC. Also, we can see stronger seasonal changes in the tide gauge stations on the eastern side of the gulf. Colors of the curves are identical to those used to mark the stations in the map to the right.

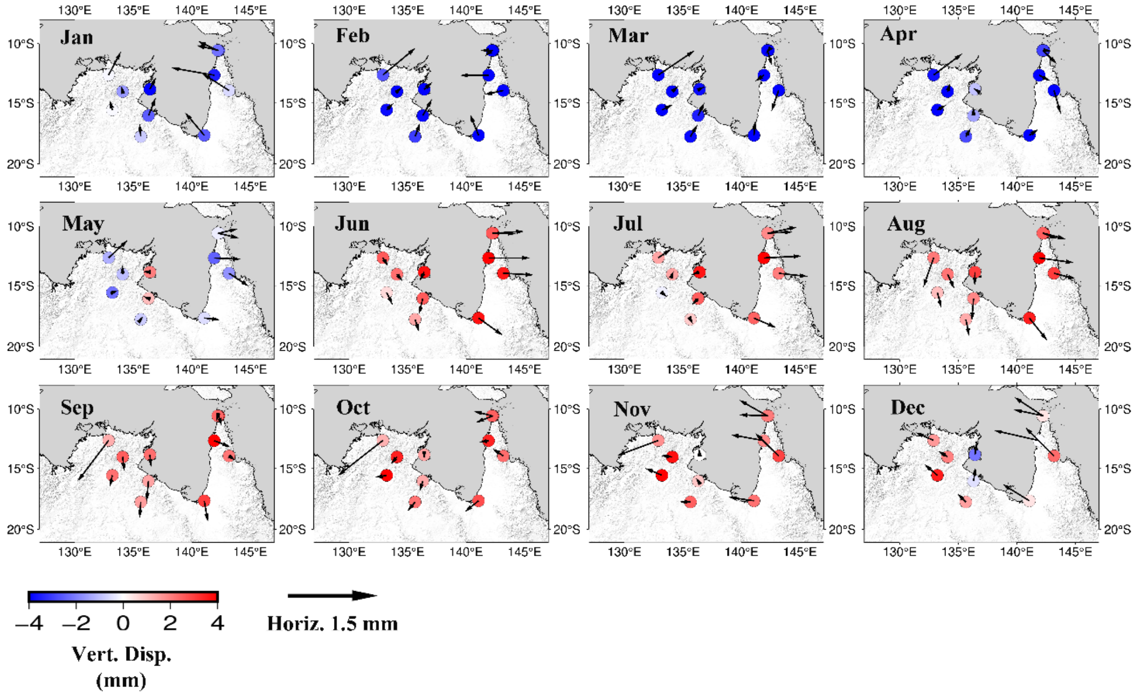

Figure S3. Observed monthly displacements in horizontal (arrows) and vertical (colors) components. They are same as those illustrated as black arrows in Figures 5.